

# Kinematic averaging effects in thermal and low energy ion-molecule collisions: Influence on product ion kinetic energy distributions

D. Gerlich

Fakultät für Physik, Universität Freiburg, D 7800 Freiburg, Germany

(Received 28 June 1988; accepted 25 August 1988)

The broadening and the shift of the kinetic energy distributions of the product ions from ion-molecule reactions caused by the velocity distributions of the reactants is discussed for different experimental situations. For a *completely thermalized system* (e.g., ions in an ideal trap) it is shown analytically that the product ion energy distribution is independent of the angular dependence of the differential cross section. In most of the cases of practical interest, the laboratory product velocity distribution for a state to state process can be approximated by a generalized Maxwell-Boltzmann distribution. Provided the exothermicity exceeds a few  $kT$ , the mean value of the corresponding energy distribution deviates from the nominal one by  $3/2kT$ , and its half width increases with the square-root of the translational exoergicity  $\Delta E_T$  i.e.,  $\text{FWHM} = (11.09 \cdot m_1' \cdot m_2' / M^2 \cdot (\Delta E_T + 1.5 \cdot kT) \cdot kT)^{1/2}$ . If the ionic and neutral reactants are *not in thermal equilibrium*, the laboratory kinetic energy becomes strongly dependent not only on the energetics but also on the differential cross section. The problem is formulated in a rather general way and then applied to different experimental methods where the product ion velocity is used directly (e.g., in KEICR, guided ion beam, and differential scattering experiments) or indirectly (e.g., in LIF experiments for the density to flux conversion) to extract information on the energetics of a collision process. The results are used to analyze recent measurements on the collision systems  $\text{N}^+ + \text{CO}$ ,  $\text{Ar}^+ + \text{CO}$ ,  $\text{Ar}^{++} + \text{He}$ , and  $\text{H}^+ + \text{D}_2$  and it will be shown that a good estimate of the total resolution function is needed for a critical analysis of experimental data.

## I. INTRODUCTION

Over the past years many experimental techniques have been developed and refined to study the partitioning of energy in chemical reactions. Various modern optical techniques can now provide state specific information but, for several reasons, they are not yet applicable to all situations and reaction systems. Therefore, the method of measuring the kinetic energy of the reaction products ("translational spectroscopy") still plays an important role due to its universality, although it can never reach the resolution of optical spectroscopy.

In the field of ion-molecule collisions additional problems arise from the low density of products, and especially from experimental difficulties in creating or detecting slow ions. Some effort has been devoted to high resolution crossed beam experiments allowing the determination of scattering angle and velocity of the emerging ions, but below 1 eV only very few results on reactive collisions have been reported until now.<sup>1-3</sup>

One of the few techniques which provides some information on the product ion kinetic energy in *thermal or near thermal* ion-molecule reactions is the KEICR (kinetic energy ion cyclotron resonance) technique pioneered by Marx *et al.*<sup>4-6</sup> and further developed by Bowers *et al.*,<sup>7-9</sup> who also tried to extend this method to hyperthermal collision energies.<sup>7</sup>

Another method has been developed in this laboratory<sup>10-13</sup> which makes use of the guided ion beam (GIB) technique, and which allows us to measure the transverse and the axial components of the product ion velocity in an octopole.

In this way low resolution differential cross sections are obtainable at energies below 100 meV; first results have been reported recently.<sup>10,11</sup> More details and results for the systems  $\text{He}^+$  and  $\text{Ar}^+ + \text{O}_2$  will be published elsewhere.<sup>12,13</sup>

However, in the KEICR and the GIB experiment, as contrasted with the rather well-defined kinematical conditions of a crossed-beam arrangement, the measured quantities consist of contributions from a wide range of initial conditions and are averaged over many final states. In addition, the analysis of the data is often handicapped by the lack of information necessary to transform from the LAB into the CM system. Substantial errors can occur in the interpretation of experimental data if one ignores the total resolution function of the apparatus. This paper provides the mathematical framework for a reliable analysis or evaluation of the laboratory velocity or energy distributions of ionic products measured in low energy ion-molecule reactions.

The averaging over quantities like the velocity and angular spread of the reactants or over the acceptance of the detector is a quite general difficulty in crossed beam, beam-cell, or bulk experiments and many investigations have been devoted to these kinds of problems.<sup>14-18</sup> The different approaches (analytical approximations, numerical simulations, integration fitting, or deconvolution procedures) depend on the goal pursued: Optimization of the construction of an apparatus designed for a special purpose, or evaluation of results obtained with a given geometry. Also, they can be grouped into different categories depending on whether one is primarily interested in the distribution of the *collision energy*,<sup>14,15</sup> or in the impairment of *angular resolution*,<sup>17,18</sup> or in the broadening of the *product energy distribution*.

This paper focuses on the last point and it is organized as follows: Subsequent to the mathematical formulation of the general problem a result for a *fully thermalized* system is obtained analytically. For some other situations (monoenergetic ions in a thermal neutral gas and ion beam-scattering cell arrangements with different detection schemes) the necessary integrals are derived. They are evaluated numerically for several examples resulting in stepwise defined apparatus functions. These functions allow a fast simulation (or deconvolution) of a measured energy distribution.

The analysis is then applied to some previous KEICR, GIB, beam-cell experiments, and also to recent LIF results because there the product laboratory velocity distribution is needed for the density to flux conversion. It will be shown that experimental results for the charge transfer from CO to  $N^+$  or  $Ar^+$ , obtained with the three methods LIF, KEICR, and GIB are in agreement within their error limits, and that some of the discrepancies discussed in the literature are due to the fact that these errors have been underestimated. Recently reported differences between beam<sup>1</sup> and KEICR<sup>4</sup> for the dissociative charge transfer  $He^+ + O_2$  will be discussed in a separate publication.<sup>12</sup> The collision systems  $H^+ + D_2$  and  $Ar^{++} + He$  are used to illustrate the broadening of the product velocity distributions in a differential beam-cell and in a GIB apparatus, respectively.

## II. BASIC FORMULAS

### A. Relation between CM and lab frame

The reactive collision of two particles forming two products is described in the usual way.<sup>19</sup> The symbols, notations, and definitions used in this paper are compiled in Table I. The transformation between the center-of-mass system (CM) and the laboratory system (LAB) is illustrated in Figs. 1(a) and 1(b) in a velocity vector representation ("Newton diagram"). For the description of experiments where the kinetic energy of the products is analyzed it is useful to introduce the quantity  $\Delta E_T$ , the translational exoergicity, i.e., the difference of the translational energies

TABLE I. Symbols and abbreviations, used in this paper. The indices 1 and 2 are related to the ion and the neutral, respectively. Primed symbols denote the corresponding values of the products (for most of the notation see also Ref. 19).

$m_1, m_2$	mass (ion, neutral)
$M = m_1 + m_2 = m'_1 + m'_2$	total mass
$\mu = m_1 \cdot m_2 / M$	reduced mass
$v_1, v_2$	velocity in the LAB frame
$g = v_1 - v_2$	relative velocity
$v_c = (m_1 v_1 + m_2 v_2) / M$	velocity of the CM of the system
$u_1 = v_1 - v_c$	velocity in the CM frame
$E_T = \mu / 2g^2$	translational or collision energy
$\Delta E_T = E'_T - E_T$	translational exoergicity
$E_I$	internal energy (vib, rot, electr.)
$-\Delta E_0$	reaction exo-ergicity
$E_1 + E_T - \Delta E_0 = E'_1 + E'_T$	total available energy
$\vartheta = \angle(u_1, u'_1)$	scattering angle (CM system)
$\phi$	azimuthal angle (CM)
$\theta = \angle(v_1, v'_1)$	scattering angle (LAB system)
$\phi$	azimuthal angle (LAB)
$\Lambda = \angle(v_1, v_2)$	intersection angle of the incident particles

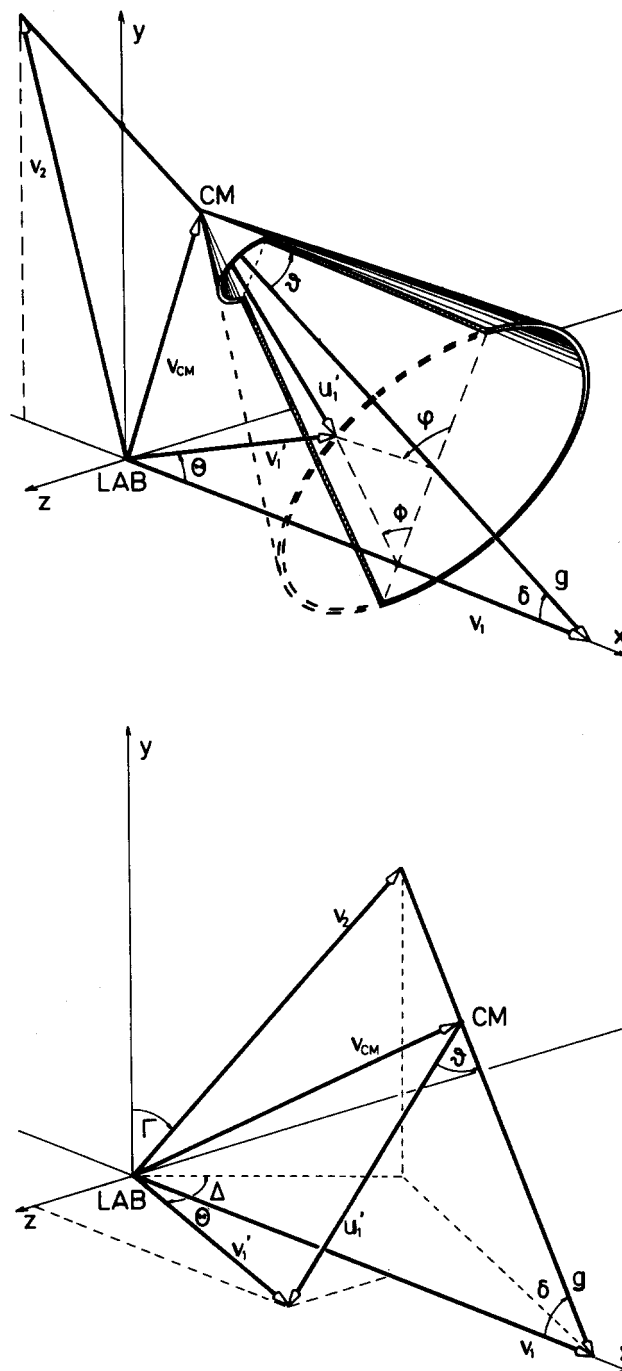


FIG. 1. Vector representation of the velocities (Newton diagram, see also Table I). The coordinate system (a) is used for the calculation of product velocity distributions  $dN(v'_1)/dv'_1$  in cases where the velocity distribution of the target molecules is rotationally symmetric relative to  $v_1$  (e.g., beam-cell arrangements, ICR cell). The collision is completely described by  $v_1, v_2$ , and  $\Lambda$ ; the product velocity  $v'_1$  is determined as soon as  $\vartheta, \phi$ , and  $\Delta E_T$  are given (Table II A). Description (b) is applied to the calculation of doubly differential product velocity distributions  $d^2N(v'_1, \theta)/d\Omega dv'_1$ , measured with an ideal differential detector in the  $xz$  plane at the angle  $\theta$ . The colliding particles are described by  $v_1, v_2, \Delta$ , and  $\Gamma$ . If  $\theta$  and  $\Delta E_T$  are given one gets two solutions (Table II B) for  $v'_1$ .

after and before the collision. Making use of energy and momentum conservation, the absolute value of the product velocity in the CM system  $u'_1$  can be calculated according to

$$u'_1 = [2(E_T + \Delta E_T)(1/m'_1 - 1/M)]^{1/2}, \quad (1)$$

and the laboratory velocity can be determined from

$$\mathbf{v}'_1 = \mathbf{v}_c + \mathbf{u}'_1 \quad (2)$$

For the calculation of laboratory product velocity distributions, suitable coordinate systems are introduced for two different experimental situations:

(1) Experimental arrangements with one axis of rotational symmetry (ICR, GIB with scattering cell) are described in the coordinate system indicated in Fig. 1(a). Without loss of generality, the initial conditions are fully determined by  $v_1$  and  $v_2$ , and  $\Lambda$ . The laboratory product ion velocity depends on  $\vartheta$ ,  $\varphi$ , and  $\Delta E_T$ . Taking the masses  $m_1$ ,  $m_2$ ,  $m'_1$ ,  $m'_2$  as fixed parameters, the velocity of the product ion  $\mathbf{v}'_1$  can be expressed as a function of six variables:

$$\mathbf{v}'_1 = \mathbf{v}'_1(v_1, v_2, \Lambda, \vartheta, \varphi, \Delta E_T) \quad (3)$$

The detailed formulas are outlined in Table II A (in a form suitable for numerical evaluations).

(2) A second situation, an experiment with an ideal differential detector, is illustrated in Fig. 1(b). The coordinate system has been chosen so that the movable detector is restricted to the  $x$ - $z$  plane, and its position is given by the LAB scattering angle  $\theta$ . Also in this case  $\mathbf{v}'_1$  can be expressed as a function (see Table II B) of a set of six parameters differing somewhat from those of Eq. (3):

$$\mathbf{v}'_1 = \mathbf{v}'_1(v_1, v_2, \Delta, \Gamma, \theta, \Delta E_T) \quad (4)$$

## B. Differential cross section

In the ideal experiment of two well collimated monochromatic beams, the number of molecules scattered per unit solid angle and per unit time is given by<sup>19</sup>

$$\frac{d\dot{N}(g, \vartheta)}{d\omega} = n_1 n_2 g \, d\tau \, d\sigma(g, \vartheta) / d\omega \quad (5)$$

Here  $n_1(\mathbf{v}_1, \mathbf{r}_1)$  and  $n_2(\mathbf{v}_2, \mathbf{r}_2)$  are the projectile and target densities in phase space, and  $d\tau$  is the scattering volume. The differential cross section  $d\sigma(g, \vartheta)$  for the state to state process  $i \rightarrow f$  (meaning a well-defined value of  $\Delta E_T$ ) depends only on the relative velocity  $g$  and the scattering angle  $\vartheta$  and is assumed to be independent of the azimuthal angle  $\varphi$  (as in

reactions of unpolarized beams). This leads to a cone of equiintensity scattering, as can be seen in Fig. 1(a). The conversion between CM and LAB intensities is straight forward for the ideal experiment,<sup>19</sup> and can be performed using the Jacobian

$$\frac{d\omega}{d\Omega} = v_1'^2 / u_1'^2 \cdot \cos^{-1}(\mathbf{u}'_1, \mathbf{v}'_1) \quad (6)$$

## III. AVERAGING PROCEDURES

In contrast to the ideal case discussed in the last chapter the kinematic conditions of a realistic experiment are less well defined, and the actually measured values are averaged over the velocities of the reactants  $\mathbf{v}_1$ ,  $\mathbf{v}_2$ , over the scattering volume  $\Delta\tau$ , and over the acceptance of the detector  $\Delta\Omega$ . Instead of Eq. (5) one obtains the 11-dimensional integral

$$\frac{d\dot{N}}{d\Omega} \Delta\Omega = \int_{\mathbf{v}_1} d\mathbf{v}_1 \int_{\mathbf{v}_2} d\mathbf{v}_2 \int_{\Delta\tau} d\tau \int_{\Delta\Omega} d\Omega \times n_1(\mathbf{r}, \mathbf{v}_1) n_2(\mathbf{r}, \mathbf{v}_2) g \frac{d\sigma}{d\omega} \frac{d\omega}{d\Omega} \quad (7)$$

$d\dot{N}/d\Omega \Delta\Omega$  is the number of all products registered per unit time by the detector (no velocity selection). The integration limits depend on the individual experimental arrangements (see below). It is easy to see that the products stem from collisions with different relative velocities  $g$  (for a discussion of the broadening of the collision energy see Refs. 14 and 15) and that for a  $\delta$ -function-like differential cross section the products are spread out over a finite angular range (for impairment of angular resolution see Refs. 17 and 18). It is also evident that the products are spread out over a range of velocities  $v'_1$ , even for a well defined state to state process. Therefore, a velocity selective detector records a distribution  $d^2\dot{N}/d\Omega \, dv'_1 \, \Delta\Omega \, \Delta v'_1$ . The determination of this function is the main purpose of this work.

In order to reduce the problem the following calculations are restricted to the influence of the velocity distributions of the reactants only. The differential detector  $\Delta\Omega$  is either assumed to be infinitesimally small or in other applications the results will be integrated over *all* angles. Also the integration over the scattering volume is simplified assuming a sufficiently small  $\Delta\tau$  (or space independent distributions) and  $n_1$  and  $n_2$  are factorized using normalized probability functions  $f_i(\mathbf{v}_i)$ ,

$$\begin{aligned} n_1(\mathbf{r}_1, \mathbf{v}_1) &= n_1(\mathbf{r}_1) f_1(\mathbf{v}_1), \\ n_2(\mathbf{r}_2, \mathbf{v}_2) &= n_2(\mathbf{r}_2) f_2(\mathbf{v}_2). \end{aligned} \quad (8)$$

With the abbreviation  $n_1 n_2 \Delta\tau = c$ , Eq. (7) may be rewritten as

$$\frac{d^2\dot{N}}{d\Omega \, dv'_1} \Delta v'_1 = c \int \int_{(\mathbf{v}_1, \mathbf{v}_2)} f_1(\mathbf{v}_1) f_2(\mathbf{v}_2) g \, d\sigma / d\omega \, d\omega / d\Omega \, d\mathbf{v}_1 d\mathbf{v}_2 \quad (9)$$

Because  $d^2\dot{N}/d\Omega \, dv'_1 \, \Delta v'_1$  denotes only the number of those products whose velocities lie in the interval  $[v'_1, v'_1 + \Delta v'_1]$  (imposed for example by a velocity sensitive detector with

TABLE II. Representation of velocity vectors in special coordinate systems [see Figs. 1(a) and 1(b), respectively].

A.	
$\mathbf{v}_1 = v_1 \cdot (1, 0, 0)$	$\mathbf{v}_2 = v_2 \cdot (\cos \Lambda \sin \Lambda, 0)$
$\mathbf{g} = \mathbf{v}_1 - \mathbf{v}_2$	
$\mathbf{v}_c = 1/M(m_1 \mathbf{v}_1 + m_2 \mathbf{v}_2 \cos \Lambda, m_2 v_2 \sin \Lambda, 0)$	
$\cos \delta = (g^2 + v_1^2 - v_2^2) / (2g v_1)$	
$u_1$ see Eq. (1)	
$u'_{1x} = u'_1 (\cos \vartheta \cos \delta + \sin \vartheta \cos \varphi \sin \delta)$	
$u'_{1y} = u'_1 (-\cos \vartheta \sin \delta + \sin \vartheta \cos \varphi \cos \delta)$	
$u'_{1z} = u'_1 (\sin \vartheta \sin \varphi)$	
$\mathbf{v}'_1 = \mathbf{v}_c + \mathbf{u}'_1$	
B.	
$\mathbf{v}_1 = v_1 \cdot (1, 0, 0)$	$\mathbf{v}_2 = v_2 \cdot (\sin \Gamma \cos \Delta, \cos \Gamma, \sin \Gamma \sin \Delta)$
$\mathbf{v}'_1 = p \pm (p^2 - v_2^2 + u_1'^2)^{1/2}$ , with	
$p = [(m_1 v_1 + m_2 v_2 \sin \Gamma \cos \Delta) \cos \theta + m_2 v_2 \sin \Gamma \sin \Lambda \sin \theta] / M$	
$\cos \vartheta = \mathbf{u}'_1 \cdot \mathbf{g} / (u'_1 g)$	

the resolution  $\Delta v'_1$ ) the integration must be limited to ranges of  $\mathbf{v}_1$  and  $\mathbf{v}_2$  where the product velocity  $v'_1$  falls into this interval. This restriction, indicated symbolically by the asterisk, can be derived in principle from the mathematical interrelation of  $\mathbf{v}'_1$ ,  $\mathbf{v}_1$ , and  $\mathbf{v}_2$  which has been shown to be practicable in a few special cases (see below). For numerical evaluation of Eq. (9), however, the computational procedure is quite simple because one needs only the dependence of  $v'_1$  from  $\mathbf{v}_1$  and  $\mathbf{v}_2$  as given by Eq. (3) or (4). An approximation of the product velocity distribution is then obtained in the form of a step function by varying  $(\mathbf{v}_1, \mathbf{v}_2)$  systematically or randomly over *all* values and by arranging the resulting particular integrands in intervals  $[v'_1, v'_1 + \Delta v'_1]$  according to the appropriate  $v'_1(\mathbf{v}_1, \mathbf{v}_2)$  (for details see Sec. III C).

#### A. Application to special experimental arrangements

Equation (9) describes quite generally the influence caused by the velocity distribution of the reactants, and can be applied to a variety of experimental situations. Some of the integrations involved can be performed analytically, others have to be evaluated numerically depending on the velocity distributions involved and on the analytical form of the cross section. The four examples (a)–(d) will be discussed briefly in the following.

(a) A first application, used here only as an illustrative example is the correlation between the *elementary integral cross section* and the measured *effective cross section*. In an ideal apparatus for measuring integral cross sections, a monoenergetic ion beam passes through a scattering cell and the products are detected with a  $4\pi$  detector.  $f_1(\mathbf{v}_1)$  is therefore a  $\delta$ -function,  $f_2(\mathbf{v}_2)$  characterizes the isotropic target gas, and the detector integrates over all angles and over all product velocities  $\mathbf{v}'_1$ . Starting from Eq. (9) one can express the signal as follows:

$$\dot{N} = cv_1 \int_{\mathbf{v}_2} g/v_1 f_2(\mathbf{v}_2) \sigma(g) d\mathbf{v}_2 = cv_1 \sigma_{\text{eff}}. \quad (10)$$

$\sigma_{\text{eff}}$ , the result of the integral, is the so-called<sup>14</sup> *effective cross section* which has been discussed in detail also by Chantray.<sup>15</sup> If  $f(\mathbf{v}_2)$  is a Maxwellian, the three-dimensional integral can be reduced analytically to an integration over the relative velocity  $g$  only.

(b) Next, Eq. (9) is used to describe experimental devices for the determination of *integral product velocity distributions*. Corresponding experimental setups must have a detector, which, on one hand, integrates over all angles but which, on the other hand, is sensitive to the absolute value of the product velocity (e.g., KEICR cell or velocity determination via Doppler shift in a bulk experiment). If the target gas is distributed isotropically the number of products registered per unit time in the velocity interval  $[v'_1, v'_1 + \Delta v'_1]$  can be calculated from

$$\begin{aligned} \frac{d\dot{N}}{dv'_1} \Delta v'_1 &= c \int_{0^*}^{\infty} dv_1 f_1(v_1) \int_{0^*}^{\infty} dv_2 f_2(v_2) \\ &\times \int_0^{\pi} g \sin \Lambda d\Lambda \int_0^{2\pi} \int_0^{\pi} d\sigma/d\omega \sin \vartheta d\vartheta d\varphi. \end{aligned} \quad (11)$$

Here, the coordinate system and angles shown in Fig. 1 (a) have been used. The function  $f_1(v_1)$  and  $f_2(v_2)$  describe the probability distribution of the absolute value of the velocities. Like in Eq. (9) the asterisk again indicates the restrictions imposed by Eq. (3) (for example, one has to bear in mind that different azimuthal angles lead to different LAB velocities  $v'_1$ ).

(c) More detailed information can be obtained with the guided beam apparatus, which allows the measurement of both the longitudinal and the transverse components of  $\mathbf{v}'_1$  with respect to  $\mathbf{v}_1$  and in this way the determination of *differential product velocity distributions*. In this case, Eq. (11) can be used, too, the only modification being the constraints imposed by Eq. (3); instead of  $v'_1$  one has to take the corresponding components of  $v'_{1t}$  (transverse to the octopole axis) or  $v'_{1p}$  (parallel) and obtains  $d\dot{N}/dv'_{1p} \Delta v'_{1p}$  or  $d\dot{N}/dv'_{1t} \Delta v'_{1t}$ , or, in analogy, one can calculate the doubly differential distribution  $d^2\dot{N}/dv'_{1p} dv'_{1t} \Delta v'_{1t} \Delta v'_{1p}$  by determining numerically a two dimensional step function.

(d) The same information can be obtained from a conventional differential scattering experiment, usually with a much better experimental resolution but with restrictions concerning energy range and sensitivity. For the calculation of the product velocity distribution caused by the target motion, the coordinates and angles shown in Fig. 1 (b) together with Eq. (4) are employed:

$$\begin{aligned} \frac{d^2\dot{N}}{d\Omega dv'_1} \Delta v'_1 &= c \int_0^{\infty} dv_1 f_1(v_1) \\ &\times \int \int \int_{(\mathbf{v}_2, \Delta\Gamma)^*} f_2(v_2, \Delta\Gamma) g d\sigma/d\omega d\omega d\Omega v_2^2 \\ &\times \sin \Gamma dv_2 d\Gamma d\Delta. \end{aligned} \quad (12)$$

Under certain conditions, Eq. (11) or (12) can be further simplified analytically. For example the three dimensional integral in Eq. (12) can be reduced to a two dimensional one by using explicitly the restraints, imposed by the relations given in Eq. (4) and Table II B.<sup>16</sup> In the following this will be done only for a completely thermalized system. In most of the situations one has to integrate numerically, some more details concerning the numerical evaluation will be given below.

#### B. Systems in thermal Equilibrium

A very special case to which Eq. (9) can be applied is the situation where the ions as well as the neutrals are completely thermalized, and where both are therefore characterized by Maxwell-Boltzmann distributions  $f_M(v_1; m_1, T)$  and  $f_M(v_2; m_2, T)$  with a common temperature  $T$ . The calculation of  $d\dot{N}/dv'_1$  can be completed analytically, and under equilibrium conditions, the product velocity distribution becomes independent on the angular dependence of the differential cross section.

This statement can be proven by replacing  $f_1(\mathbf{v}_1)$  and  $f_2(\mathbf{v}_2)$  in Eq. (9) by Maxwell-Boltzmann distributions with a common temperature  $T$ . The laboratory velocities  $\mathbf{v}_1$  and  $\mathbf{v}_2$  have to be substituted by  $\mathbf{v}_c$  and  $\mathbf{g}$ . Making use of the

relations given in Table I, replacing  $m_1/2 v_1^2 + m_2/2 v_2^2$  by  $\mu/2 g^2 + M/2 v_c^2$ , and after some calculation one obtains

$$\frac{d\dot{N}}{dv_1'} \Delta v_1' = c \int_{\mathbf{g}} f_M(\mathbf{g}; \mu, T) \mathbf{g} \sigma(\mathbf{g}) \left\{ \int_{\mathbf{v}_c} f_M(\mathbf{v}_c; M, T) d\mathbf{v}_c \right\} d\mathbf{g} \quad (13)$$

The individual steps are omitted, because this result can be derived more directly if one uses the following fact: If the velocity distributions of any arbitrarily selected pair of particles 1 and 2 are both independent Maxwell-Boltzmann distributions  $f_M(v_1; m_1, T)$  and  $f_M(v_2; m_2, T)$ , then  $f_M(v_c; M, T)$  and  $f_M(\mathbf{g}; \mu, T)$ , the distribution of the center-of-mass velocity of this pair and the distribution of its relative velocity, are independent Maxwell-Boltzmann distributions, too. This is easy to prove in Cartesian coordinates, because it is sufficient to show this relation in one dimension due to the statistical independence of the Cartesian components.

From this statement it is evident that for all arbitrarily selected relative velocities  $\mathbf{g}$  one gets the same isotropic distribution of  $\mathbf{v}_c$ , there is no correlation between the product velocity  $\mathbf{u}_1'$  and  $\mathbf{v}_c$ , and therefore the resulting  $v_1'$  distribution must be independent on the differential cross section.

This independence of  $f_M(v_c; M, T)$  and  $f_M(\mathbf{g}; \mu, T)$  leads also directly to Eq. (13) by taking into account that the probability for a collision is proportional to  $g \cdot \sigma(\mathbf{g})$ , and that the integration over  $\mathbf{v}_c$  is limited by the condition (again symbolized by the asterisk) that the product velocity falls into the interval  $[v_1', v_1' + \Delta v_1']$ .

This last restriction can be taken into account analytically. The mathematical derivation is in all details analogous to the treatment of Chantry (see Fig. 1 of Ref. 15 and also Ref. 20) although the problem treated there is somewhat different. Briefly, the condition  $v_1' \leq |\mathbf{v}_c + \mathbf{u}_1'| \leq v_1' + \Delta v_1'$  is fulfilled for all those  $\mathbf{v}_c$  for which the laboratory velocity vector ends in a shell of a sphere with radius between  $v_1'$  and  $v_1' + \Delta v_1'$ . Integration of  $f_M(v_c; M, T)$  over this volume can be carried out and simplifies Eq. (13) to:

$$d\dot{N}/dv_1' = c \int_{\mathbf{g}} g \sigma(\mathbf{g}) f_M(\mathbf{g}; \mu, T) f^*(v_1', \mathbf{u}_1'; T) d\mathbf{g}, \quad (14)$$

where  $f^*$  is the generalized Maxwell-Boltzmann distribution

$$f^*(v_1', \mathbf{u}_1'; T)$$

$$= (M/2\pi kT)^{1/2} \frac{v_1'}{u_1'} \left\{ \exp\left[-\frac{M}{2kT} (v_1' - u_1')^2\right] - \exp\left[-\frac{M}{2kT} (v_1' + u_1')^2\right] \right\}. \quad (15)$$

For numerical analysis it is convenient to introduce dimensionless velocities and energies:

$$\hat{u}_1' = u_1' \left\{ \frac{2kT}{M} \right\}^{-1/2}, \quad \hat{v}_1' = v_1' \left\{ \frac{2kT}{M} \right\}^{-1/2}, \\ \hat{g} = g \left\{ \frac{2kT}{\mu} \right\}^{-1/2}, \quad \hat{E}_1' = E_1' \left\{ \frac{m_1'}{M} kT \right\}^{-1}, \quad (16)$$

and one gets the result:

$$d\dot{N}/d\hat{v}_1' = c \int_0^\infty \hat{g} \sigma(\hat{g}) f_M(\hat{g}) \cdot f^*(\hat{v}_1', \hat{u}_1'; T) d\hat{g} \quad (17)$$

with the two Maxwell-Boltzmann functions in the following dimensionless formulation:

$$f_M(\hat{g}) = 4\pi^{-1/2} \hat{g}^2 \exp(-\hat{g}^2), \quad (18)$$

$$f^*(\hat{v}_1', \hat{u}_1'; T) = \pi^{-1/2} \hat{v}_1'/\hat{u}_1' \{ \exp[-(\hat{v}_1' - \hat{u}_1')^2] - \exp[-(\hat{v}_1' + \hat{u}_1')^2] \}. \quad (19)$$

The mean value of the product energy  $\langle E_1' \rangle$  is calculated from Eq. (14):

$$\langle E_1' \rangle = m_1'/2 \langle v_1'^2 \rangle \\ = m_1'/2 \int_0^\infty v_1'^2 d\dot{N}/d\hat{v}_1' d\hat{v}_1' / \int_0^\infty d\dot{N}/d\hat{v}_1' d\hat{v}_1' \\ = (\Delta E_T + kT \langle \hat{g}^2 \rangle) \frac{m_2'}{M} + \frac{3}{2} kT \frac{m_1'}{M}, \quad (20)$$

the mean value of  $\hat{g}^2$  being dependent on the cross section  $\sigma(\mathbf{g})$ :

$$\langle \hat{g}^2 \rangle = \int_0^\infty \hat{g}^5 \sigma(\hat{g}) \exp(-\hat{g}^2) d\hat{g} \\ \times \int_0^\infty \hat{g}^3 \sigma(\hat{g}) \exp(-\hat{g}^2) d\hat{g}. \quad (21)$$

It must be emphasized that all results derived so far have been obtained without any approximation, the only requirement which must be met is the complete thermalization of the reactants. For further analysis some approximations are needed. In the following we assume that the cross section  $\sigma(\mathbf{g})$  is proportional to  $g^{-1}$  (Langevin cross section). From Eq. (21) we obtain  $\langle \hat{g}^2 \rangle = 3/2$  and for the mean value of the product kinetic energy the very simple result:

$$\langle E_1' \rangle = m_2'/M \Delta E_T + 1.5 kT. \quad (22)$$

A further analytical simplification of the distribution  $d\dot{N}/dv_1'$  (Eq. 17) is handicapped by the fact that  $f^*(\hat{v}_1', \hat{u}_1'; T)$  is an implicit function of  $\hat{g}$ , because using the dimensionless variables, Eq. (1) may be written:

$$\hat{u}_1' = \left( \hat{g}^2 + \frac{\Delta E_T}{kT} \right) \frac{m_2'}{m_1'}. \quad (23)$$

However, for most practical applications it is sufficient to replace  $\hat{u}_1'^2$  by its mean value replacing  $\hat{g}^2$  by  $\langle \hat{g}^2 \rangle$ :

$$\hat{E}_0' = \langle \hat{u}_1'^2 \rangle = \left( \langle \hat{g}^2 \rangle + \frac{\Delta E_T}{kT} \right) \frac{m_2'}{m_1'}, \quad (24)$$

$$E_0' = \frac{m_2'}{M} \left( \Delta E_T + \frac{3}{2} kT \right).$$

With this approximation and with  $\sigma(\mathbf{g}) \sim g^{-1}$ , integration of Eq. (17) leads to the following product ion velocity distribution:

$$d\dot{N}/d\hat{v}_1' = C \pi^{-1/2} \hat{v}_1' \hat{E}_0'^{-1/2} \{ \exp[-(\hat{v}_1' - \hat{E}_0'^{1/2})^2] - \exp[-(\hat{v}_1' + \hat{E}_0'^{1/2})^2] \}. \quad (25)$$

The new constant  $C$  contains  $c = n_1 n_2 \Delta \tau$  and the proportional factor of  $\sigma \sim 1/g$ . Substituting  $\hat{v}_1'^2$  by  $\hat{E}_1'$  we obtain the corresponding product ion energy distribution:

$$d\dot{N}/d\hat{E}_1' = c (4\pi \hat{E}_0')^{-1/2} \{ \exp[-\hat{E}_1'^{1/2} - \hat{E}_0'^{1/2}]^2 - \exp[-(\hat{E}_1'^{1/2} + \hat{E}_0'^{1/2})^2] \}. \quad (26)$$

For  $\hat{E}'_1 \gg 1$  the second exponential term can be neglected, and Eq. (26) becomes a Gaussian function peaking at  $\hat{E}'_1 = \hat{E}'_0$  (shifted relative to the mean laboratory energy  $\langle \hat{E}'_1 \rangle$ ) and having full width at half maximum (FWHM) of:

$$\begin{aligned} [\hat{E}'_1]_{1/2} &= (16 \ln 2 \hat{E}'_0)^{1/2} \text{ or} \\ [E'_1]_{1/2} &= (11.09 \frac{m'_1 \cdot m'_2}{M^2} (\Delta E_T + \frac{3}{2} kT) kT)^{1/2}. \end{aligned} \quad (27)$$

From a mathematical point of view, these results are very similar to the well-known formula for the "Doppler broadening in beam experiments" derived by Chantry<sup>15</sup> as can be seen from a comparison between our Eq. (26) and Eq. (9) of Ref. 15. However the subject is different, Chantry is concerned with the influence of the thermal target motion on the distribution of collision energies while our results are dealing with the impairment of product velocities. In both cases the superposition of velocities leads to an at first sight unexpected broad distribution.

A very close relation exists between Eq. (25) and the velocity distribution of ions formed via photo- or electron dissociation. The distributions for such cases have been derived by Chantry and Schulz<sup>20</sup> superimposing the velocity of the mother molecule and the relative velocities of the fragments.

At the end of this chapter it must be emphasized again, that Eq. (25) is only valid for  $\sigma(g) \sim g^{-1}$  while for other situations (e.g., low energy threshold) Eq. (17) has to be evaluated numerically. The important result that the energy distribution depends only on the integral cross section and not on the angular dependence needs only the condition of a completely thermalized system. If this is not fulfilled, information on the energetics of a reaction process can not be obtained without the knowledge of the differential cross section as will be demonstrated below.

### C. Numerical considerations

It has already been mentioned that for a further evaluation of Eq. (9) [respectively, Eq. (11) and (12)] one has to determine that subspace of the integration limits ( $\mathbf{v}_1, \mathbf{v}_2$ ) for which the product velocities fall into the interval  $[v'_1, v'_1 + dv'_1]$ . In principle the necessary relations can be derived by an adequate transformation of the formulas, given in Table II. However, it cannot be expected that one obtains generally such simple analytical solutions like Eq. (13) for a fully thermalized system and for the final evaluation numerical methods are needed anyway for most of the problems. Therefore, for all other experimental situations, treated in this work, Eq. (11) or (12) have been evaluated numerically.

We have made the experience that for the given problem, Monte Carlo methods are inferior to a systematic variation of the variables. A few representative angles and several sample velocities  $v_1$  and  $v_2$  [selected according to the weighting functions  $f_i(v_i)$ ] are sufficient for the determination of the product energy distribution.

The variation of all variables runs over the full range

without any restriction. In order to account for the constraints imposed by Eq. (3) or (4) (and indicated by the asterisk) not only the integrand  $I(\mathbf{v}_1, \mathbf{v}_2)$  must be calculated for each sample point but also the product velocity  $v'_1(\mathbf{v}_1, \mathbf{v}_2)$  using the equations of Table II. The value of the integrand is then added to a variable of a field  $N(\nu)$  where the integer  $\nu$  is determined from the condition  $\nu \cdot \Delta v'_1 \leq v'_1(\mathbf{v}_1, \mathbf{v}_2) < (\nu + 1) \cdot \Delta v'_1$ . The interval  $\Delta v'_1$  has to be chosen according to the required resolution. This procedure leads directly to a numerical approximation of  $d\dot{N}/dv'_1$  in the form of the step function  $N(\nu)/\Delta v'_1$ . For the determination of doubly differential distributions the data are stored in a two-dimensional field.

Some problems arise from the fact that the dependence of the differential cross section  $d\sigma/d\omega$  on the relative velocity  $g$  and on the scattering angle  $\vartheta$  are often unknown, some consequences of which will be illustrated in the next paragraph. Generally the velocity dependence of  $d\sigma/d\omega$  can be approximated with that of the integral cross sections (from measurements or using the Langevin cross section). The angular dependence has been dealt with in two ways. In certain cases formation of a long lived complex has been assumed ( $d\sigma/d\vartheta = \text{const}$ ). More generally, the  $\vartheta$  dependence is approximated by a set of  $\delta$  functions:

$$d\sigma_i/d\omega = \delta(\vartheta - \vartheta_i)/(2\pi \sin \vartheta_i). \quad (28)$$

With these, and several values for  $\Delta E_T$  and  $E_T$ , the numerical evaluation of the integral leads to a set of apparatus functions  $F(v'_1; \vartheta_i, \Delta E_{Tj}, E_{Tk})$ , and any product distribution can be expanded as a sum over such functions

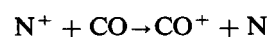
$$d\dot{N}/dv'_1 = \sum_{ijk} \alpha_{ijk} F(v'_1; \vartheta_i, \Delta E_{Tj}, E_{Tk}) \quad (29)$$

allowing a fast simulation (or deconvolution) of measured velocity distributions.

If many functions  $F$  have to be superimposed it has been proven useful to approximate the numerical results by analytical functions facilitating the further processing of the data. If one uses Gaussians, only a very few sample points (50–100) are needed to determine the mean value, the standard deviation, and the norm of the distribution.

### IV. APPLICATION TO EXPERIMENTAL DATA

In the following, the results of the previous section are applied to some specific examples. Several charge transfer processes and reactions have been chosen, which have been examined at thermal and low kinetic energies using different experimental arrangements (ICR, LIF, guided beam, beam-cell). The primary aim of the analysis is to demonstrate the influence of the thermal motion and of the differential cross section on the product energy distributions, and to illustrate the resulting limitations of the techniques. A detailed discussion of the consequences for the interpretation of the particular reactions is outside the scope of the present paper.



The exothermicity of the charge transfer from CO to

$N^+$  ( $\Delta E_0 = -0.52$  eV) allows the formation of vibrationally and rotationally excited products. These state distributions have been studied by the technique of laser-induced fluorescence in an ion-beam apparatus at an average collision energy of 0.13 eV<sup>21</sup> and later in a flowing after glow apparatus at 300 K thermal energy.<sup>23</sup> Some apparent contradictions to beam experiments, performed at 0.5 eV in this laboratory,<sup>22</sup> could be explained with the poorly known angular distribution of the  $CO^+$  products and the influence of the thermal motion of the target gas.

Recently, also the technique of kinetic energy ion cyclotron resonance spectroscopy (KEICR) has been used to study this reaction.<sup>7</sup> Some variation of collision energy from thermal up to several tenths of an eV was achieved by selective translation excitation of the ions. As usual for KEICR measurements, the raw data have been plotted as the percentage of trapped product ions against the square root of the trapping voltage  $V_T$ , one example [thermal conditions, Fig. 2(a) from Ref. 7] is reproduced in Fig. 3. The formation on the product kinetic energy is extracted from the break in the curve and [especially at higher energies, see Figs. 2(a) and 2(c) in Ref. 7] from the intercept of the linearly extrapolated part at  $V_T = 0$ . Although the extracted vibrational state distributions and their dependence on the collision energy are in qualitative accordance with very recent LIF results,<sup>24</sup> this evaluation method is made doubtful and uncertain due to the thermal broadening and due to kinematic influences. The following numerical examples show, that the break is in reality a smooth bend (even for a single value of  $\Delta E_T$ ), and

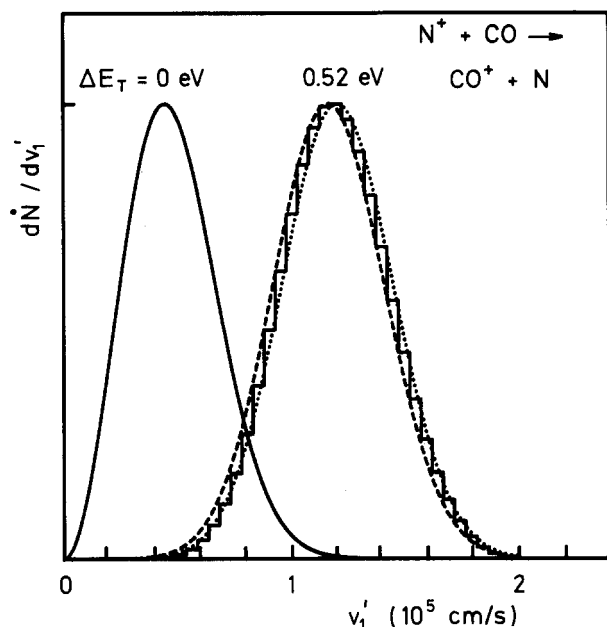


FIG. 2. Velocity distributions of  $CO^+$  products formed in a thermal charge transfer process; if no reaction energy is transferred into translation ( $\Delta E_T = 0$  eV) the result is a usual Maxwellian. For  $\Delta E_T = 0.52$  eV three curves are compared: The dotted and dashed line shows  $dN/dv_1$ , given by Eq. (25), for the dashed line the term  $3/2kT$  has been omitted in  $\hat{E}'_0$  [Eq. (24)]. The step function has been calculated by direct numerical integration of Eq. (11).

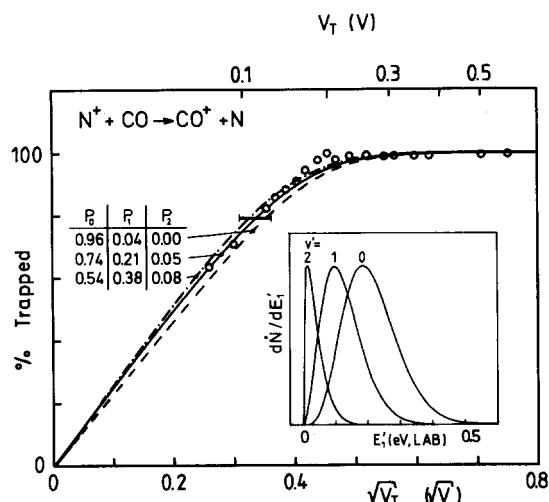


FIG. 3. Fraction of  $CO^+$  ions trapped in the ICR cell vs the square root of the trapping voltage. Dots: experimental values from Ref. 7, Fig. 2(a); error bar: calibration of the  $V_T$  scale ( $\pm 20$  meV). The insert shows  $CO^+(v)$  product energy distributions for excitation of  $v = 0-2$ ; the broadening is exclusively due to the thermal motion. The trapping curves ("break curves") have been calculated for the three sets of  $P_0$  shown in the figure and are all in accord with the ICR data.

that under certain conditions the extrapolation method can lead to erroneous results.

Figure 2 shows calculated velocity distributions of  $CO^+$  ions produced by the  $N^+ + CO$  charge transfer with  $\Delta E_T = 0$  and 0.52 eV. If no translational energy is gained in the reaction it is obvious that the product velocity distribution is a usual Maxwell-Boltzmann distribution and it is easy to show, that Eq. (25) reverts to the usual Maxwellian for  $\Delta E_T \rightarrow 0$ . For  $\Delta E_T = 0.52$  eV, three curves are compared. The dotted line shows  $dN/dv_1$  determined from the analytically derived function [Eq. (25)] while the step function is the result of the numerical integration of Eq. (11), replacing  $f_1(v_1)$  and  $f_2(v_2)$  by Maxwell-Boltzmann distributions, assuming  $d\sigma/d\omega \sim 1/(g \cdot \sin \vartheta)$ , and using a rather coarse interval for  $\Delta v_1$ . By reduction of  $\Delta v_1$  and increasing the number of integration points, this function approximates the generalized Maxwell-Boltzmann distribution with any desired accuracy. The dashed curve has been calculated from Eq. (25) by neglecting the contribution of  $3/2kT$  in  $\hat{E}'_0$  to  $\Delta E_T$  resulting in a significant shift (compare also a and d in Table III).

TABLE III. Mean values of the kinetic energy  $\langle E'_1 \rangle$  and FWHM of the distributions for  $N^+ + CO \rightarrow CO^+ + N$  assuming  $\Delta E_T = -\Delta E_0 = 0.52$  eV (units are eV).

	a	b	c	d
$\langle E'_1 \rangle$	0.1733	0.2120	0.2060	0.2121
FWHM	0	0.1887	0.1867	0.1886

<sup>a</sup> Nominal values ( $T = 0$  K).

<sup>b</sup> Numerically determined using the Langevin cross section.

<sup>c</sup> Same as b, however using the experimental cross section from Ref. 22.

<sup>d</sup> Analytical approximations Eqs. (20) and (27) ( $T = 300$  K).

The influence of the  $g$  dependence of the differential cross section has been treated more realistically by replacing the Langevin cross section with the experimentally known energy dependence of the integral cross section ( $\sigma = \min\{23.5 \cdot E^{-0.5}, 1.45 \cdot E^{-1.2}\}$ , units are  $\text{\AA}^2$  and eV, see Ref. 22). As a consequence, the mean value of the product energy  $\langle E_1' \rangle$  is shifted, however, only by 6 meV (compare b and c in Table III). For other cross sections (e.g., low energy thresholds), stronger deviations must be expected.

Table III shows also that all numerically obtained half-widths are all in good agreement with the value determined with the analytical approximation Eq. (27). This indicates that Eq. (25) describes in good approximation the product velocity distribution for the  $N^+ + CO$  charge transfer at thermal conditions. Therefore, and for simplicity and reproducibility, this approximation [or Eq. (26) for the calculation of energy distributions] will be used in the following analysis of the ICR experiment.

Some thermally broadened distributions for the formation of  $CO^+$  ( $v = 0, 1, \text{ and } 2$ ) are shown in the insert of Fig. 3, in this case as a function of the energy. The examples illustrate that the FWHM of the energy distributions increases with the translational exothermicity [see Eq. (27)] complicating the precise determination of the product internal excitation. In order to calculate the fraction of ions which are stored in the ICR cell for various vibrational populations (see  $P_0, P_1,$  and  $P_2$  in Fig. 3, rotation is ignored for simplicity) the corresponding energy distributions have been integrated, according to the trapping conditions.<sup>4,5</sup> The resulting three curves (Fig. 3) demonstrate that the thermal broadening washes out the breaks. Comparison with the experimental results from Ref. 7 reveals that a much better signal-to-noise ratio would be necessary to discern the remaining slight differences between the three assumed populations. An additional problem is the precise calibration of the real trapping potential (contact and surface potentials), and already an uncertainty of only 20 meV (error bar in Fig. 3) impedes the distinction of a relatively large range of possible vibrotational distributions of the  $CO^+$  product (for a discussion of other examples see below).

The situation becomes even less favorable if the ions are *not in thermal equilibrium with the neutrals*. In addition to the thermal broadening, caused by the neutral target molecules, the product energy distributions become strongly dependent on the scattering angle and an evaluation of the energy distributions without any knowledge of the differential cross section becomes impossible. In order to illustrate the consequences, product velocity distributions have been calculated for monoenergetic  $N^+$  ions (0.1 eV) reacting with thermal CO neutrals: the function  $f_1(v_1)$  in Eq. (11) is replaced by a  $\delta$  function,  $f_2(v_2)$  by a Maxwell-Boltzmann distribution, and the differential cross section has been taken as  $\delta$  functions peaking at  $\vartheta = 0^\circ, 60^\circ, 120^\circ,$  or  $180^\circ$ . The obtained distributions show (see Fig. 4 and compare with Fig. 2) that the backward scattered ions are much slower than the forward scattered products.

This result becomes more obvious in Fig. 5 where the mean value of the product kinetic energy,  $\langle E_1' \rangle$  is plotted as a function of  $E_1$ , the LAB kinetic energy of the reacting ions

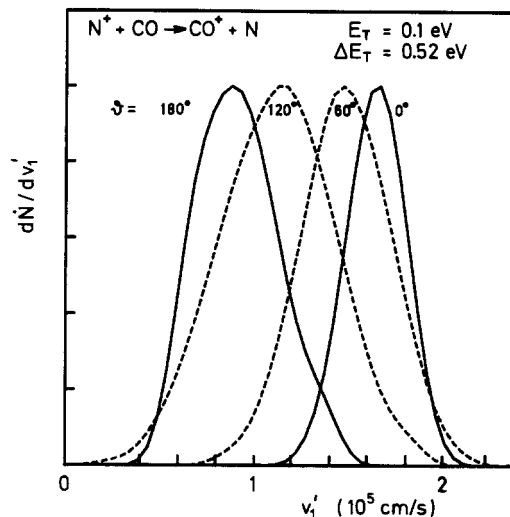


FIG. 4. The  $CO^+$  product velocity distributions [obtained by numerical integration of Eq. (11)] for the charge transfer between monoenergetic  $N^+$  ions and thermal CO target depend strongly on the scattering angle.

for several scattering angles. Comparison of the dashed  $T = 0$  K curves (nominal values) with the 300 K results reveals a significant shift caused by the thermal motion, especially in the backward direction. The curves for the different angles cut all each other only for one energy ( $E_1 \sim kT$ ), otherwise the product ion energy depends strongly on  $\vartheta$  and that is on the differential cross section.

This impedes the analysis of energy distributions, measured under nonthermal conditions, if one lacks some

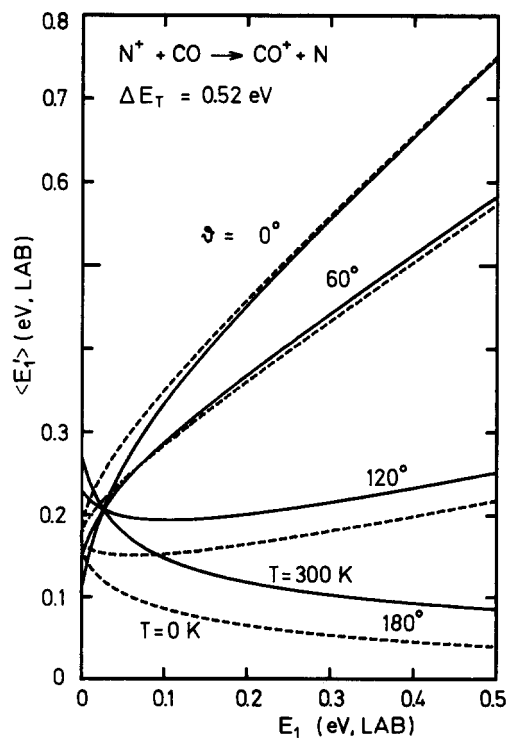
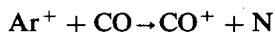


FIG. 5. Mean value of the laboratory product energy  $E_1'$  vs laboratory energy  $E_1$  of the  $N^+$  ions for different scattering angles (thermal target,  $T = 300$  K). Nominal values ( $T = 0$  K) are plotted as dashed lines.

knowledge about the differential cross section. Therefore, the detection of decreasing product energy with increasing collision energy (like in Ref. 7) doesn't allow the conclusion that the internal excitation becomes enhanced because this observation is as well in agreement with a preference of backward scattering; even if the full exothermicity is converted into translation, the products can lose kinetic energy in the LAB frame.

Considering the KEICR experiment, several conclusions can be drawn from the preceding example: The method is unsuitable to give reliable evidence on energy partitioning for nonthermal reactants, but it can provide important information under thermal conditions. In order to extract this information in the case of *slow products*, it is recommended to analyze the measured break curves with a convolution (or deconvolution) procedure and not with the simple extrapolation method. In the case of *large translational exoergicity*  $\Delta E_T$  (see for example Ref. 29) the mean value of the product energy is almost unaffected by the thermal distributions [the contribution  $1.5 \cdot kT$  is negligible in Eq. (23)], however, one should not expect a sharp break; according to Eq. (27) the energy resolution becomes increasingly worse. The consequence is that also in this situation usually rather different energy distributions lead to trapping curves which are in accord with the data points. Depending on the signal-to-noise ratio, it is therefore advisable to simulate or to deconvolute the experimental results, based on Eq. (26). The situation of multiple breaks will be discussed in Ref. 12.



The charge transfer  $\text{Ar}^+ + \text{CO} \rightarrow \text{CO}^+ + \text{Ar}$  is 1.74 eV exothermic. From ICR experiments<sup>5,27</sup> a rather narrow translation energy distribution has been deduced, peaking at  $\Delta E_T = 0.56$  eV, and suggesting that the major part of the  $\text{CO}^+$  ions appears in the  $v = 4$  vibrational state. Also for this charge transfer process, laser-induced-fluorescence experiments have been carried out<sup>25,26</sup> and it has been shown that the  $\text{CO}^+(v)$  distribution is indeed inverted with the maximum at  $v = 5$  (see Table IV); however, it is rather broad and all accessible states are populated with significant probabilities. The disagreement between the ICR and LIF results has been qualitatively discussed in Ref. 26. The following more detailed analysis of the ICR and the LIF signals, taking only into account the thermal spread in reagent velocities, reveals some of the sources of the discrepancies. Some recent GIB results will be included.

The ICR results of Ref. 5 are reproduced in Fig. 6. As described above, the ICR results have been simulated [based on Eq. (26)] making different assumptions for the internal excitation. At first sight, the curve calculated for  $\Delta E_T = 0.56$  eV (excitation of  $v = 4$  only) is in very good overall agreement with the data. However, there is a discrepancy concerning the half widths of the distributions. The FWHM of the calculated energy distribution shown in the insert of Fig. 6 is 0.204 eV [Eq. (27)], while the FWHM extracted from the experiment in Ref. 5 is specified with 0.07 eV. Because our analysis of the experiment accounts exclusively for the thermal broadening and is therefore a lower limit, this can only be due to an optimistic interpretation of a few data

TABLE IV. Relative vibrational population probabilities (in %) for  $\text{Ar}^+ + \text{CO} \rightarrow \text{CO}^+(v_1) + \text{Ar}$ . I) LIF, beam results, collision energy about 0.2 eV (Ref. 25). a: relative values before speed corrections, b: vibrational population with error limits, taken from Tab. II of Ref. 25. II) Vibrational populations (evaluation of this work) using different assumptions concerning the differential cross section and taking into account the thermal broadening; a: isotropic scattering, b: only forward scattering, c: only backward scattering; d:  $v = 3$  backward,  $v = 4 - 7$  forward scattered. The italic numbers are the mean product velocities in  $10^5$  cm/s. III) LIF, thermal conditions (flowing afterglow experiment, Ref. 26).

$v$	I		II				III
	a	b	a	b	c	d	
0	1.6	$7_{-5}^{+5}$	3 2.9	2 3.7	4 2.1	1 2.1	$6 \pm 4$
1	2.2	$5_{-4}^{+5}$	3 2.7	3 3.5	5 1.9	2 1.9	$7 \pm 2$
2	5.1	$9_{-4}^{+6}$	7 2.5	7 3.3	9 1.7	4 1.7	$9 \pm 2$
3	6.0	$10_{+8}^{+10}$	8 2.3	7 3.1	9 1.4	4 1.4	$15 \pm 3$
4	11.7	$15_{-6}^{+7}$	14 2.1	13 2.8	15 1.2	15 2.8	$21 \pm 3$
5	31.8	$31_{-4}^{+4}$	32 1.8	32 2.5	31 0.9	35 2.5	$27 \pm 2$
6	37.8	$20_{-9}^{+6}$	31 1.5	33 2.2	25 0.6	36 2.2	$15 \pm 2$
7	3.8	$3_{-2}^{+6}$	2 1.1	3 1.6	2 0.5	3 1.6	...

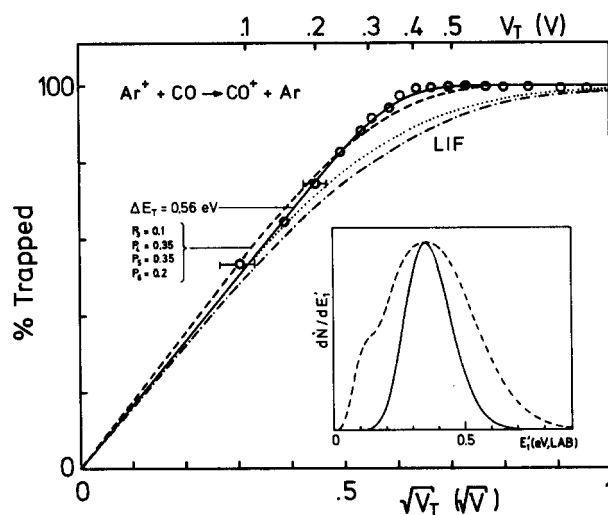


FIG. 6. Fraction of  $\text{CO}^+$  ions trapped in the ICR cell vs the square root of the trapping voltage. Dots: experimental results from Ref. 5; error bars: calibration of the  $V_T$  scale ( $\pm 20$  meV). The ICR data are in good agreement with the simulation for  $\Delta E_T = 0.56$  eV ( $P_4 = 1$ ); however, a wider vibrational population ( $P_3 = 0.1$ ,  $P_4 = 0.35$ ,  $P_5 = 0.35$ ,  $P_6 = 0.2$ ) also results in a curve (dashed line) lying within the experimental error bars. The corresponding energy distributions are shown in the insert. The deviations from the LIF results (dotted line: beam experiment (Ref. 25),  $E_T = 0.2$  eV, dash-dotted line: flowing afterglow Ref. 26, populations see Table IV) are discussed in the text.

points deviating slightly from our calculated curve in the region of the break.

In addition, the instrumental resolution can lead to further broadening and there is some uncertainty in the calibration of the energy scale (the bars indicate an assumed error of 20 meV). Furthermore, a nonthermal primary ion distribution can lead to significant distortions, as discussed in the previous section (see also Fig. 7). For these reasons the ICR results do not allow the conclusion that only a narrow distribution of  $\text{CO}^+$  states is excited in the charge transfer process. In fact the data are, within their error limits, also in agreement with a much wider vibrational distribution as demonstrated with the dashed curve in Fig. 6 where  $v = 3-6$  has been assumed to be excited with the probabilities  $P_v$  printed in the figure.

In this way a major part of the disagreement between the ICR and the LIF experiments can be explained by the thermal broadening limiting the energy resolution of the ICR method. However, some discrepancies remain outside of our estimates of the error limits. This becomes evident from the dotted and dash-dotted lines in Fig. 7 which have been calculated with the populations, determined by LIF<sup>25,26</sup> (see Table IV). This deviation is due to the contributions of the low vibrational states, leading to large translational energies. Possible explanations are: nonthermal ion distributions in the ICR cell, vibrational relaxation in the flowing afterglow LIF experiment, or erroneous speed correction factors in the LIF beam experiment. The last point will be discussed in more detail in the following.

The evaluation of the beam LIF experiment is affected by the insufficiently known product velocity distribution because the measured relative light intensities are proportional to the product density rather than to the desired quantity, the product flux (see also the discussion in Refs. 21 and 25). Correction factors accounting for the laboratory product ion energy are therefore needed. In Ref. 25 this speed correction was based on the assumption, that the spatial velocity distribution in the center-of-mass frame is isotropic, however the thermal target motion has been neglected.

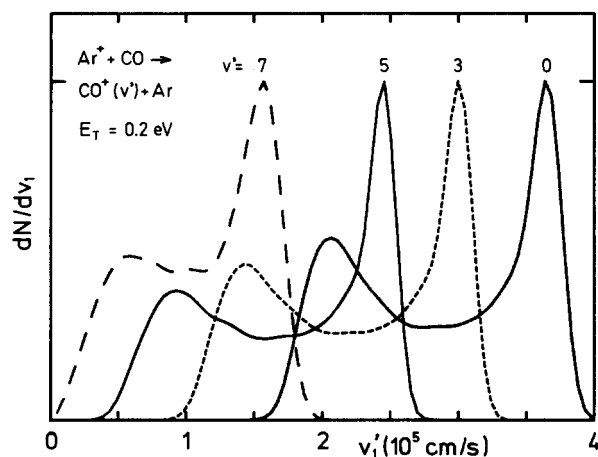


FIG. 7. Typical  $\text{CO}^+$  product velocity distributions needed for correcting the LIF results from Ref. 25.

The product velocity distribution calculated from Eq. (11) has been used to reevaluate the LIF data, in the course of which several assumed differential cross sections have been tested. For isotropic scattering  $d\sigma/d\vartheta = \text{const}$  the  $\text{CO}^+$  ( $v = 0, 3, 5,$  and  $7$ ) velocity distributions are shown in Fig. 7. All other results are compiled in Table IV, column II. The mean values of the product ion velocities  $\langle v_1' \rangle$  are printed in italics. Correction of the raw LIF data (Column Ia) with these factors leads to vibrational distributions deviating somewhat from the published values, however, most of the population probabilities are still within the error limits given by Lin *et al.*<sup>25</sup> (column Ib). One exception is the  $v = 6$  state which is more favored in our evaluation mainly at the expense of the lower vibrational states 0-3. This difference indicates that it is necessary to use the thermally averaged instead of the nominal ( $T = 0$ ) velocities especially if the products become slow.

The two extreme assumptions that all  $\text{CO}^+$  products are forward or backward scattered lead to quite different product velocities (Table IV, columns II b and c), but the distributions are only slightly shifted to higher or lower vibrational states, respectively. A somewhat larger change is obtained, if one assumes that the  $\text{CO}^+$  ( $v = 0-3$ ) are backward and the others forward scattered leading to a significant suppression of the low vibrational states. This shows that for a more definitive evaluation of the LIF data some more information on the product angular distribution is needed.

As a third method, besides LIF and KEICR, the guided ion beam technique has been applied to the exploration of energy partitioning in this charge transfer process. So far, only product velocity distributions  $dN/dv_{1p}$  (velocity component parallel to the octopole axis) have been measured by time of flight, a strong enough guiding field ensuring integration over all transverse velocities  $v_{1t}$ . One example for a collision energy of 35 meV is plotted in Fig. 8.

The distribution peaks at very low velocities being indicative for a strong internal excitation of the  $\text{CO}^+$  products

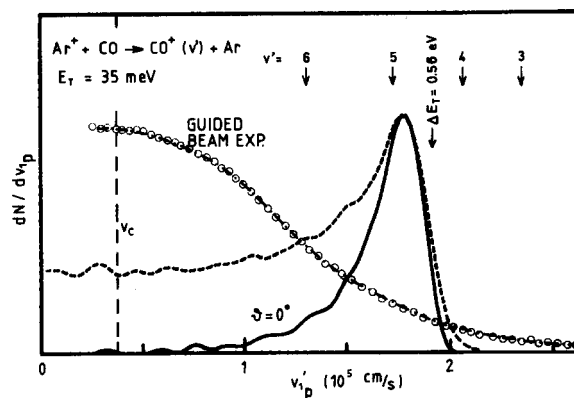
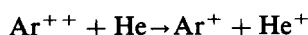


FIG. 8.  $\text{CO}^+$  product  $v_{1p}$  distributions (component of  $v_1'$  parallel to  $v_1$ ). Dots: GIB data. Simulations are shown for  $\Delta E_T = 0.56$  eV, and for  $d\sigma/d\vartheta = \text{const}$  (dashed line) and for  $d\sigma/d\vartheta = \delta(\vartheta = 0^\circ)$  (heavy line). The arrows mark the nominal velocities  $v_1'$  of the  $\text{CO}^+$  ion if the corresponding vibrational state is excited.

( $v = 5$  and  $6$ ) in qualitative accordance with the LIF data. However, for a more quantitative analysis, the transverse product velocity and the backward scattered part must be analyzed. Corresponding work is in progress.

For comparison with the result, extracted from the ICR data, Eq. (11) has been used to simulate the GIB velocity distribution for a sharp  $\Delta E_T$  distribution peaking at  $0.56$  eV ( $v = 4$ ). In one case (solid line) forward scattering has been assumed, in the other case isotropic scattering (dashed line). The results give some idea about the resolution achievable in the GIB experiment. It is evident that the assumption, that only  $v = 4$  gets excited, is in no case compatible with our data.



The charge transfer from  $\text{He}(^1S)$  to  $\text{Ar}^{++}(^3P)$  is  $3.1$  eV exothermic. Because at low kinetic energies no excited states are energetically accessible (ignoring the nonresolvable fine structure), the translational exoergicity is well defined. This makes it possible to obtain state specific information even with a medium resolution apparatus, or to resolve relative contributions of various electronic states of the reactant ion.<sup>28</sup>

From a practical point of view this reaction is well suited for testing the angular and energy resolution of an experimental method, and it has been used, therefore, to characterize a differential scattering guided ion beam apparatus.<sup>10,11</sup> A detailed analysis of this method has shown that the overall resolution is mainly limited by the thermal broadening if one uses a beam-cell arrangement.

$\text{Ar}^+$  product velocity distributions  $dN/dv'_{ip}$  have been calculated for the above mentioned charge transfer applying Eq. (11) and using the experimentally determined energy dependence of the integral cross section.<sup>11</sup> Inspection of the Newton diagram shows, that all  $\text{Ar}^+$  products are forward scattered in the LAB frame regardless of the CM scattering angle, and that for this simple state to state process the distribution  $dN/dv'_{ip}$  already contains the full information on the differential cross section.

The angular dependence of the cross section has been approximated by a series of  $\delta$  functions peaking at different scattering angles. Three examples in Fig. 9(a) ( $\vartheta = 0^\circ, 90^\circ,$  and  $180^\circ$ , dotted lines) show that the resulting thermally broadened velocity distributions are rather narrow in the forward and backward direction while sideward scattering leads to a broader distribution. The other examples in Fig. 9(a) show that for a differential cross section  $d\sigma/d\vartheta \sim \sin \vartheta$  the experimentally observable curve becomes trapezoidal while for  $d\sigma/d\vartheta = \text{const}$  the forward and backward peaks are dominant.

Measured data have been fitted with a sum of such distributions, the weights giving directly the deconvoluted information on the differential cross section. One example is shown in Fig. 9(b) where an experimental  $\text{Ar}^+$  velocity distribution is compared with a simulated one. The resulting differential cross section has been reported and discussed already in Refs. 10 and 11. For the purpose of the present paper it is important to note, that the good agreement proves that the thermal target motion causes the major part of the

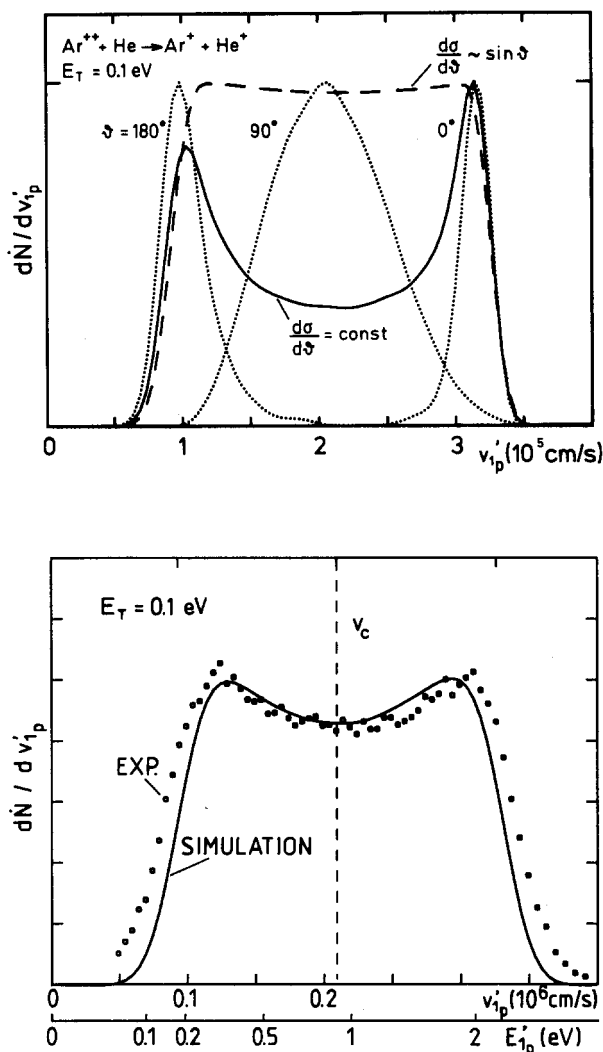
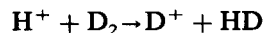


FIG. 9.  $\text{Ar}^+$  product  $v'_{ip}$  distributions (component of  $v'_i$  parallel to  $v_i$ ); a: simulation of distributions for different differential cross sections  $d\sigma/d\vartheta$ ; b: Comparison: GIB data-simulation, details see Ref. 10 and 11.

broadening. The remaining differences are due to other experimental averaging effects (length of the scattering cell, time resolution) not included in the present simulation.



As a last example of the influence of the target motion on the product translational energy, an ideal differential scattering apparatus is treated (monoenergetic, well collimated ion beam, detector with perfect angular and velocity resolution), the only disadvantage being the thermal random velocity distribution of the target gas.

It has been shown experimentally with a less ideal realization of such an apparatus<sup>3</sup> that for some reaction systems advantageous kinematic conditions allow the partial resolution of single rotational states. One example, the proton-deuteron exchange in  $\text{H}^+ + \text{D}_2$  collisions, is reproduced in Fig. 10(a). The measured distribution extends over a wide range of product kinetic energies and features some structure indicative of excitation to a variety of rotational states. The de-

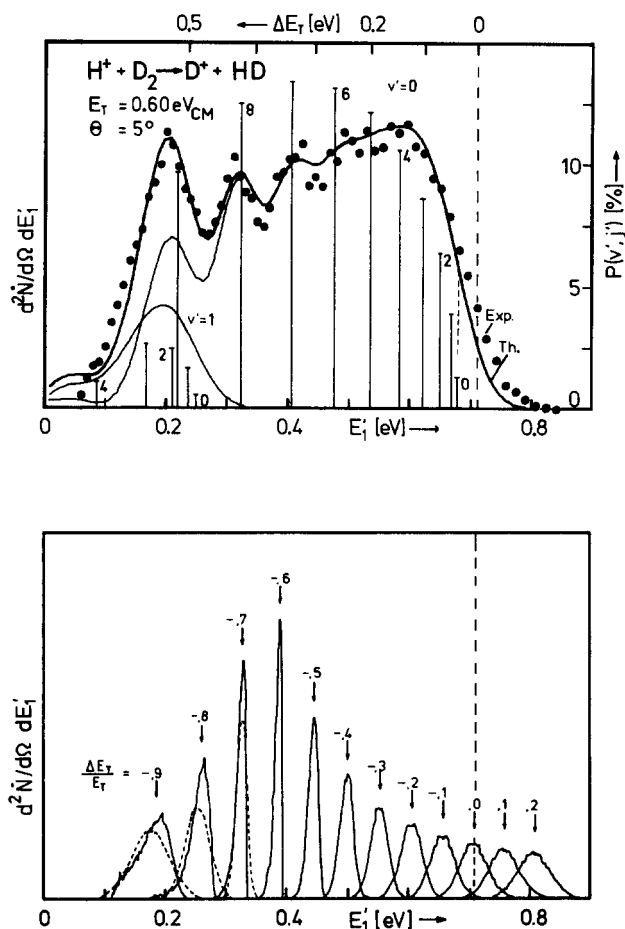


FIG. 10. Differential energy distributions of  $D^+$  products, formed in  $H^+ + D_2$  collisions at  $E_T = 0.6$  eV and observed at a laboratory scattering angle of  $\theta = 5^\circ$ . a: Experimental points of Ref. 3, the bars indicate the extracted population probabilities  $P(v = j')$  (scale at right), the line shows a simulation, accounting for the overall resolution of the apparatus. b: Numerical results of Eq. (12): influence of the target motion (80 K scattering cell) assuming an otherwise ideal apparatus.

convoluted results, the excitation probabilities  $P(v'j')$ , are indicated as bars. The solid line shows the simulated distribution, convoluting these probabilities with  $F_T(E_1'; \theta, \Delta E_T)$ , the overall resolution function of the apparatus. This function combines the influence of the energy spread of the ion beam, the resolution of the detector and the influence of the target motion approximating the individual contributions by Gaussian functions. The influence of the thermal broadening will be discussed in more detail in the following.

The experimental situation is illustrated in Fig. 1(b). For a given LAB scattering angle  $\theta$  and a translational exoergicity  $\Delta E_T$  the product velocity distributions have been calculated from Eq. (12). The differential cross section has been approximated assuming  $d\sigma/d\omega = 1/(g \sin \vartheta)$  irrespective of the product state. Numerical integration is carried out by systematic variation of  $v_2$ ,  $\Delta$ , and  $\Gamma$ . In the experiment, the target gas was cooled to liquid nitrogen temperature, therefore the calculations have been performed for  $T = 80$  K.

Some product energy distributions are plotted in Fig. 10(b) for selected relative translational exoergicities  $\Delta E_T/E_T$  [the distributions for  $\Delta E_T(v_j)$  are derived by interpolation, facilitating the evaluation at higher energies where too many states are accessible]. It can be seen that for this example (mass ratio, etc.) the thermal motion causes the smallest broadening, if about 2/3 of the translational energy is converted into internal excitation; under favorable conditions focusing effects can compensate for the thermal broadening.

The functions can be approximated with sufficient accuracy by Gaussians (dotted lines) for further processing and it is worthwhile to note that the determination of the parameters characterizing these Gaussian functions (accuracy a few percent) needs less than 100 integration points ( $v_2, \Delta, \Gamma$ ). Comparison of Fig. 10(a) with Fig. 10(b) reveals that for this example, full resolution of the rotational states  $j' = 6, 7$ , and 8 would be possible with a scattering cell if all other experimental averaging effects could be avoided.

## CONCLUSIONS

The general problem of averaging over different parameters arises in all practical cases of nonideal scattering experiments. In this paper one special aspect has been treated—the influence of the target motion on the product kinetic energy. It has been shown that a fully thermalized system is an exceptional case where the mean value of the product energy distribution is independent from the angular behavior of the differential cross section. Analytical formulas for the calculation of this mean value and of the often very large halfwidth of this distribution have been derived.

For nonthermal systems the mathematical framework has been supplied for calculating the product energy distributions, and the formulas have been evaluated numerically for some special experimental conditions. In all cases the target molecules have been assumed to be thermalized and spatially isotropic. It is, however, no problem to apply the described method to other problems, for example to the numerical exact treatment of crossed or merged beam arrangements.

With these results, some published experimental data for a few low energy ion-molecule reactions have been reanalyzed. It has been shown that in certain cases rather erroneous conclusions are possible if one disregards the thermal motion of the target gas. It has been shown as well that medium resolution differential cross sections are obtainable with a beam cell arrangement. This is especially important for low energy ion-molecule reactions, where the other methods are not yet applicable or where the differential cross sections are needed for the evaluation of data obtained with optical methods.

## ACKNOWLEDGMENTS

The author is grateful to Ch. Schlier for his continuous interest and helpful advice. Thanks are due to R. Marx and D. C. Parent for having stimulated part of this work and for several suggestions. Concerning the general treatment of the subject, fruitful discussions with E. Tely are acknowledged.

- <sup>1</sup>G. Bischof and F. Linder, *Z. Phys. D* **1**, 303 (1986).
- <sup>2</sup>J. M. Farrar, in *Techniques for the Study of Ion-Molecule Reactions*, edited by J. M. Farrar and W. H. Saunders, Jr. (Wiley, New York, 1988).
- <sup>3</sup>E. Teloy in *Electronic and Atomic Collisions*, edited by G. Watel (North-Holland, Amsterdam, 1978), p. 591; and D. Gerlich, Ph. D. thesis, Feiburg, Germany, 1977.
- <sup>4</sup>G. Mauclaire, R. Derai, S. Fenistein, and R. Marx, *J. Chem. Phys.* **70**, 4017 (1979).
- <sup>5</sup>R. Marx, in *Ionic Processes in the Gas Phase*, edited by M. A. Almoester Ferreira (Reidel, Boston, 1984), p. 67.
- <sup>6</sup>D. Parent, R. Derai, G. Mauclaire, M. Heninger, R. Marx, M. Rincon, A. O'Keefe, and M. Bowers, *Chem. Phys. Lett.* **117**, 127 (1985).
- <sup>7</sup>A. O'Keefe, D. Parent, G. Mauclaire, and M. T. Bowers, *J. Chem. Phys.* **80**, 4901 (1984).
- <sup>8</sup>A. O'Keefe, G. Mauclaire, D. Parent, and M. T. Bowers, *J. Chem. Phys.* **84**, 215 (1986).
- <sup>9</sup>M. Rincon, J. Pearson, and M. Bowers, *Int. J. Mass Spectrom. Ion Phys.* **80**, 133 (1987).
- <sup>10</sup>D. Gerlich, in *Electronic and Atomic Collisions*, edited by D. C. Lorents, E. E. Mayerhof, and J. R. Peterson (Elsevier, Amsterdam, 1986), p. 541.
- <sup>11</sup>R. Disch, S. Scherbarth, and D. Gerlich, in *Conference on the Dynamics of Molecular Collisions*, edited by D. G. Truhlar and P. J. Dagdigian (Snowbird, Utah, 1985), p. 20 C; (to be published).
- <sup>12</sup>D. Gerlich, S. Scherbarth, and M. Schweizer (to be published).
- <sup>13</sup>D. Gerlich and S. Scherbarth (to be published).
- <sup>14</sup>K. Berkling, R. Helbing, K. Kramer, H. Pauly, Ch. Schlier, and P. Toschek, *Z. Phys.* **166**, 406 (1962).
- <sup>15</sup>P. J. Chantry, *J. Chem. Phys.* **55**, 2746 (1971).
- <sup>16</sup>E. Teloy (private communication).
- <sup>17</sup>R. Düren, Max-Planck-Institut für Strömungsforschung, Göttingen, Report 12 (1977).
- <sup>18</sup>M. Shapiro, R. B. Gerber, U. Buck, and J. Schleusener, *J. Chem. Phys.* **67**, 3570 (1977).
- <sup>19</sup>R. D. Levine and R. B. Bernstein, *Molecular Reaction Dynamics* (Oxford University, Oxford, 1974).
- <sup>20</sup>P. J. Chantry and G. J. Schulz, *Phys. Rev.* **156**, 134 (1967).
- <sup>21</sup>D. R. Guyer, L. Hüwel, and S. R. Leone, *J. Chem. Phys.* **79**, 1259 (1983).
- <sup>22</sup>D. Gerlich, in *Symposium on Atomic and Surface Physics*, edited by F. Howorka, W. Lindinger, and T. D. Märk (Institut für Atomphysik der Universität Innsbruck, Salzburg, 1984), pp. 116-121.
- <sup>23</sup>C. E. Hamilton, V. M. Bierbaum, and S. R. Leone, *J. Chem. Phys.* **83**, 601 (1985).
- <sup>24</sup>G. H. Lin, J. Maier, and S. R. Leone, *J. Chem. Phys.* **84**, 2180 (1986).
- <sup>25</sup>G. H. Lin, J. Maier, and S. R. Leone, *J. Chem. Phys.* **82**, 5527 (1985).
- <sup>26</sup>C. E. Hamilton, V. M. Bierbaum, and S. R. Leone, *J. Chem. Phys.* **83**, 2284 (1985).
- <sup>27</sup>R. Marx, G. Mauclaire, and R. Derai, *Int. J. Mass Spectrom. Ion Phys.* **47**, 155 (1983).
- <sup>28</sup>B. Friedrich and Z. Herman, *Chem. Phys. Lett.* **107**, 375 (1984).
- <sup>29</sup>M. Rincon, J. Pearson, and M. Bowers, *Int. J. Mass Spectrom. Ion Phys.* **80**, 133 (1987).